One-Step Persymmetric GLRT for Subspace Signals

Jun Liu, *Senior Member, IEEE*, Siyu Sun, and Weijian Liu, *Member, IEEE*

***Abstract*—We exploit persymmetric structures to design a generalized likelihood ratio test for detecting subspace signals in homogeneous Gaussian clutter with unknown covariance matrix. The subspace model is employed to account for mismatches in the target steering vector. An exact but finite-sum expression for the probability of false alarm of the proposed detector is derived, which is verified using Monte Carlo simulations. This expression is irrelevant to the clutter covariance matrix, indicating that the proposed detector exhibits a constant false alarm rate property against the clutter covariance matrix. Numerical examples show that the proposed detector has strong robustness to the target steering vector mismatch.**

***Index Terms*—Adaptive detection, persymmetry, subspace signal, constant false alarm rate, generalized likelihood ratio test.**

I. Introduction

MULTICHANNEL radar target detection in Gaussian clutter has been a topic of long-standing interest [1]–[7]. As customary, one often imposes a standard assumption that a set of training (secondary) data is available for the estimation of clutter covariance matrix. In radar applications, training data are collected from the vicinity of the cell under test. Kelly did pioneering work in [8], where he designed a generalized likelihood ratio test (GLRT) detector for the adaptive detection problem. Importantly, the GLRT detector has a constant false alarm rate (CFAR) property against the clutter covariance matrix. Note that this GLRT detector was designed using the one-step method. Specifically, all the unknown parameters were estimated by using both the test and training data together. Another way to design an adaptive detector is the two-step approach, where a test statistic is obtained in the first step by assuming the clutter covariance matrix is known, and then the maximum likelihood (ML) estimate of the clutter covariance matrix based on the training data is employed to take the place of the true clutter covariance matrix in the test statistic obtained in the first step. Using such a two-step method, Robey *et al.* developed an adaptive matched filter (AMF) detector [9] which is computationally more efficient than Kelly's GLRT detector. In addition, the AMF also exhibits the CFAR property with respect to the clutter covariance matrix.

Note that the GLRT in [8] and AMF in [9] were designed for the case of rank-one signal where the target steering vector is assumed known up to a scalar. In practice, there may exist a mismatch in the target steering vector due to beam-pointing errors and multipath [10]. To account for the uncertainty in the target steering vector, a subspace model is widely used in open literature [11]–[19]. More specifically, in the subspace model the target signal is expressed as the product of a known full-column-rank matrix and an unknown column vector. It means that the target signal lies in an known subspace spanned by the columns of a matrix, but its exact location is unknown since the coordinate vector is unknown. More detailed explanations about the subspace model can be found in [11], [12], [14].

In [14], several matched subspace detectors were developed in Gaussian clutter, where the clutter covariance matrix is assumed known. The authors in [20] designed a one-step GLRT detector for detecting subspace signals when the clutter covariance matrix is unknown. For ease of reference, this detector is called SGLRT detector hereafter. The SGLRT detector was also applied to polarimetric target detection [21]. A two-step GLRT detector for subspace signal, also referred to as subspace adaptive matched filter (SAMF), was proposed in [22], [23]. The analytical performance of the SGLRT and SAMF detectors was provided in [23]. An adaptive subspace detector (ASD) was proposed in [15] where a scaling factor was introduced for accounting for the power mismatch between the test and training data. The ASD was adopted for detecting stochastic subspace signals in [16] and [17]. In [18], [19], several adaptive detectors were designed for detecting double subspace signals.

As pointed out in a rule of thumb [24], the number of homogeneous training data is required to be about twice the data dimension to achieve satisfactory performance. In practice, this requirement on the training data size may be prohibitive due to outliers and variations in terrain types. Note that all the work mentioned above does not exploit clutter covariance matrix structures (except Hermitian). Actually, one can exploit *a priori* knowledge about the clutter covariance matrix structure to alleviate the requirement on the number of training data.

In practice, Hermitian persymmetric structure exists in clutter covariance matrix, when a radar receiver employs a symmetrically spaced linear array and/or symmetrically spaced pulse trains [25]–[32]. Hermitian persymmetry indicates that the clutter covariance matrix is Hermitian about its principal

Manuscript received November 6, 2018; revised March 11, 2019 and May 15, 2019; accepted May 15, 2019. Date of publication May 24, 2019; date of current version June 7, 2019. The associate editor coordinating the review of this manuscript and approving it for publication was Dr. Fabiola Colone. This work was supported in part by the National Natural Science Foundation of China under Grants 61871469 and 61771442, in part the Youth Innovation Promotion Association CAS under Grant CX2100060053, in part the Fundamental Research Funds for the Central Universities under Grant WK2100000006, and in part the Key Research Program of the Frontier Sciences, CAS, under Grant QYZDY-SSW-JSC035. *(Corresponding author: Weijian Liu.)*

J. Liu and S. Sun are with the Department of Electronic Engineering and Information Science, University of Science and Technology of China, Hefei 230027, China (e-mail: jun_liu_math@hotmail.com; junliu@ustc.edu.cn).

W. Liu is with the Wuhan Electronic Information Institute, Wuhan 430019, China (e-mail: liuvjian@163.com).

Digital Object Identifier 10.1109/TSP.2019.2918994

diagonal, and persymmetric about its cross diagonal. Hereafter, "persymmetric" always means "Hermitian persymmetric" for brevity. It was proven in [33] that the exploitation of persymmetry is to double the number of training data, and hence brings in obvious performance gains.

In [34], Cai and Wang exploited the persymmetry to design a GLRT detectors for rank-one signals in multiband radar. For ease of reference, this detector is referred to as Cai-Wang's GLRT. The two-step GLRT detector exploiting persymmetry was provided for detecting rank-one signals in [35], [36], whose performance was analyzed in [37]. The existing work on persymmetric adaptive detection mostly focuses on the rank-one signal case. To the best of our knowledge, very limited work is conducted on the subspace signal detection by exploiting persymmetry. In [38], the authors proposed a tunable detector for detecting subspace signals by employing persymmetry. Approximate expressions for the probability of false alarm and detection probability were obtained in an intuitive way. This tunable detector involves a two-step persymmetric GLRT detector for subspace signals as a special case [38, eq. (14)]. However, a one-step GLRT exploiting persymmetry for subspace signal detection has not been derived yet.

In this paper[1], we exploit persymmetry to propose a one-step GLRT for subspace signal detection in Gaussian clutter with unknown covariance matrix. Remarkably, an exact yet simple expression for the probability of false alarm of the proposed detector is derived, which indicates the constant false alarm rate (CFAR) against the clutter covariance matrix. The theoretical expression is verified using the standard Monte Carlo (MC) simulation. Numerical examples are provided to illustrate that the proposed detector exhibits strong robustness to the mismatches in the target steering vector, at the price of a performance loss in the matched case. It is worth noting that the steering vector is assumed known in [28], [37], [39], whereas we take into consideration the steering vector uncertainties, and adopt a subspace model to propose the one-step GLRT detector with improved robustness in this study.

The remainder of this paper is organized as follows. In Section II, the data model is introduced, and the problem of interest is formulated. The one-step GLRT is proposed by exploiting persymmetry in Section III. In Section IV, a finite-sum expression for the probability of false alarm is derived. Numerical examples are provided in Section V, and we make conclusions in Section VI.

II. Problem Formulation

Assume that the data under test are collected from N (temporal, spatial, or spatial-temporal) channels. We examine the problem of detecting the presence of a point-like target. The echoes from the range cell under test, called primary or test data, are denoted by

$$\mathbf{x} = \mathbf{\Sigma}\mathbf{a} + \mathbf{n}, \tag{1}$$

where $\mathbf{\Sigma} \in \mathbb{C}^{N\times q}$ is a known target subspace matrix[2], $\mathbf{a} \in \mathbb{C}^{q\times 1}$ is an unknown complex coordinate vector accounting for the target reflectivity and channel propagation effects, and $\mathbf{n}$ denotes clutter in the range cell under test. Suppose that the clutter $\mathbf{n}$ has a circularly symmetric, complex Gaussian distribution with zero mean and covariance matrix $\mathbf{R}_p \in \mathbb{C}^{N\times N}$, i.e., $\mathbf{n} \sim \mathcal{CN}(\mathbf{0}, \mathbf{R}_p)$.

As customary, a set of secondary (training) data $\{\mathbf{y}_k\}_{k=1}^K$ free of the target echoes is assumed available, i.e.,

$$\mathbf{y}_k = \mathbf{n}_k \sim \mathcal{CN}(\mathbf{0}, \mathbf{R}_p), \tag{2}$$

for $k = 1, 2, \ldots, K$. Suppose further that the clutter $\mathbf{n}$ and $\mathbf{n}_k$s for $k = 1, 2, \ldots, K$ are independent and identically distributed (IID). In radar applications, these training data are collected from the cells adjacent to the cell under test.

Let the valid hypothesis (H_1) and null hypothesis (H_0) be that the target echoes are present and absent in the test data, respectively. The target detection problem at hand can be cast to the following binary hypothesis test

$$H_0 : \begin{cases} \mathbf{x} \sim \mathcal{CN}(\mathbf{0}, \mathbf{R}_p), \\ \mathbf{y}_k \sim \mathcal{CN}(\mathbf{0}, \mathbf{R}_p),\ k = 1, 2, \ldots, K, \end{cases} \tag{3a}$$

$$H_1 : \begin{cases} \mathbf{x} \sim \mathcal{CN}(\mathbf{\Sigma}\mathbf{a}, \mathbf{R}_p), \\ \mathbf{y}_k \sim \mathcal{CN}(\mathbf{0}, \mathbf{R}_p),\ k = 1, 2, \ldots, K, \end{cases} \tag{3b}$$

where $\mathbf{a}$ and $\mathbf{R}_p$ are both unknown. In the open literature, several adaptive detectors have been developed for the above detection problem (3), such as the SGLRT [20], [21], [44], SAMF [22], [23], and ASD [15], [17]. Note that these existing subspace detectors do not take into consideration any covariance matrix structures (except Hermitian).

In practice, the covariance matrix $\mathbf{R}_p$ has a persymmetric structure, when the receiver uses a symmetrically spaced linear

[1] *Notation*: Vectors (matrices) are denoted by boldface lower (upper) case letters. Superscripts $(\cdot)^T$, $(\cdot)^*$ and $(\cdot)^\dagger$ denote transpose, complex conjugate and complex conjugate transpose, respectively. $\mathbb{C}^{m\times n}$ and $\mathbb{R}^{m\times n}$ are complex and real matrix spaces of dimension $m \times n$, respectively. $\mathbf{I}_n$ stands for an identity matrix of $n \times n$, and $\mathbf{0}_{m\times n}$ represents a null matrix of dimension $m \times n$. For notational simplicity, we sometimes drop the explicit indexes in $\mathbf{I}_n$ and $\mathbf{0}_{m\times n}$ if no confusion exists. The notation $\sim$ means "be distributed as", $\mathcal{CN}(\boldsymbol{\mu}_c, \mathbf{R}_c)$ denotes a circularly symmetric, complex-valued Gaussian distribution with mean $\boldsymbol{\mu}_c$ and covariance matrix $\mathbf{R}_c$, $\mathcal{N}(\boldsymbol{\mu}_r, \mathbf{R}_r)$ represents a real-valued Gaussian distribution with mean $\boldsymbol{\mu}_r$ and covariance matrix $\mathbf{R}_r$, $\mathcal{W}_n(m, \mathbf{R})$ denotes the n-dimensional real-valued Wishart distribution with m degrees of freedom and scale matrix $\mathbf{R}$. The $n \times m$ matrix $\mathbf{C} = [\mathbf{c}_1, \mathbf{c}_2, \ldots, \mathbf{c}_m] \sim \mathcal{N}(\mathbf{0}_{n\times m}, \mathbf{R} \otimes \mathbf{I}_m)$ means that the column vectors $\mathbf{c}_j$ are independent identically distributed (IID) as $\mathbf{c}_j \sim \mathcal{N}(\mathbf{0}_{n\times 1}, \mathbf{R})$ for $j = 1, 2, \ldots, m$. $\otimes$ is the Kronecker product. $|\cdot|$ represents the modulus of a scalar and the determinant of a matrix, when the argument is a scalar and matrix, respectively. $\mathfrak{Re}$ and $\mathfrak{Im}$ represent the real and imaginary parts of a complex quantity, respectively. $F_{n,m}$ is a real central F-distribution with n and m degrees of freedom. χ^2_n denotes a real central Chi-squared distribution with n degrees of freedom, while $\chi'^2_n(\zeta)$ denotes a real non-central Chi-squared distribution with n degrees of freedom and a non-centrality parameter ζ. $\Gamma(\cdot)$ is the Gamma function, and $\mathrm{C}_n^m = \frac{n!}{m!(n-m)!}$ is the binomial coefficient. $\mathbb{C}^m$ and $\mathbb{R}^m$ denote m-dimensional complex and real vector spaces, respectively. $\lceil\cdot\rceil$ denotes the smallest integer greater than or equal to a given number. $\mathrm{tr}(\cdot)$ denotes the trace of a matrix, and $\jmath = \sqrt{-1}$.

[2] The subspace target model is widely used for improving the robustness to signal mismatch [12], [15], [20], [40]. In practice, we can construct the subspace matrix $\mathbf{\Sigma}$ by using the nominal steering vector and the ones close to the nominal steering vector [10], [41]–[43], to take into account the uncertainty in the target steering vector.

array and/or symmetrically spaced pulse trains [25], [34]. When $\mathbf{R}_p$ is persymmetric, it satisfies

$$\mathbf{R}_p = \mathbf{J}\mathbf{R}_p^*\mathbf{J}, \tag{4}$$

where

$$\mathbf{J} = \begin{bmatrix} 0 & 0 & \cdots & 0 & 1 \\ 0 & 0 & \cdots & 1 & 0 \\ \vdots & \vdots & \vdots & \vdots & \vdots \\ 0 & 1 & \cdots & 0 & 0 \\ 1 & 0 & \cdots & 0 & 0 \end{bmatrix}_{N\times N}. \tag{5}$$

We assume that the target subspace matrix $\mathbf{\Sigma}$ is persymmetric, which means that $\mathbf{\Sigma} = \mathbf{J}\mathbf{\Sigma}^*$. Note that this persymmetric assumption on $\mathbf{\Sigma}$ is exploited for the derivations of robust GLRT detector.

It has to be pointed out that the persymmetric structures imposed on $\mathbf{R}_p$ and $\mathbf{\Sigma}$ make the detection problem considered here different from that in [20]. Moreover, under the persymmetric assumption, the authors in [38] examined the detection problem (3) by first transforming the received data with a unitary matrix such that the persymmetric matrices $\mathbf{\Sigma}$ and $\mathbf{R}_p$ become real-valued. Then, a tunable detector was proposed, which includes two important adaptive detectors as special cases: the PAMF and persymmetric ASD designed with the two-step method. Approximate expressions for the probability of false alarm and detection probability were obtained in an intuitive way. It has to be emphasized that no detector is designed in [38] according to the one-step method.

In the following, we propose a one-step GLRT detector by exploiting the persymmetry. Moreover, an exact but finite-sum expression for the probability of false alarm is derive. For mathematical tractability, we assume that $K \geq \lceil \frac{N}{2} \rceil$ in the detection problem (3). This is a more interesting and also practically motivated case. This constraint is much less restrictive than the one (i.e., $K \geq N$) required in [20], [17], [15].

III. One-Step GLRT

In this section, we incorporate the persymmetry to design the GLRT detector according to the one-step method, namely,

$$\Lambda_1 = \frac{\max_{\{\mathbf{a},\mathbf{R}_p\}} f_1(\mathbf{x},\mathbf{y}_1,\ldots,\mathbf{y}_K)}{\max_{\{\mathbf{R}_p\}} f_0(\mathbf{x},\mathbf{y}_1,\ldots,\mathbf{y}_K)} \underset{H_0}{\overset{H_1}{\gtrless}} \lambda_1, \tag{6}$$

where λ_1 is a detection threshold, $f_1(\mathbf{x},\mathbf{y}_1,\ldots,\mathbf{y}_K)$ and $f_0(\mathbf{x},\mathbf{y}_1,\ldots,\mathbf{y}_K)$ denote the joint probability density functions (PDFs) of the primary and secondary data under H_1 and H_0, respectively. Due to the independence among the primary and secondary data, $f_1(\mathbf{x},\mathbf{y}_1,\ldots,\mathbf{y}_K)$ can be written as

$$f_1(\mathbf{x},\mathbf{y}_1,\ldots,\mathbf{y}_K) = \left\{ \frac{1}{\pi^N|\mathbf{R}_p|} \exp\left[-\mathrm{tr}(\mathbf{R}_p^{-1}\mathbf{T}_1)\right] \right\}^{K+1}, \tag{7}$$

where

$$\mathbf{T}_1 = \frac{1}{K+1}\left[(\mathbf{x}-\mathbf{\Sigma}\mathbf{a})(\mathbf{x}-\mathbf{\Sigma}\mathbf{a})^\dagger + \tilde{\mathbf{R}}_p \right] \tag{8}$$

with $\tilde{\mathbf{R}}_p = \sum_{k=1}^K \mathbf{y}_k\mathbf{y}_k^\dagger$. In addition, $f_0(\mathbf{x},\mathbf{y}_1,\ldots,\mathbf{y}_K)$ can be expressed by

$$f_0(\mathbf{x},\mathbf{y}_1,\ldots,\mathbf{y}_K) = \left\{ \frac{1}{\pi^N|\mathbf{R}_p|} \exp\left[-\mathrm{tr}(\mathbf{R}_p^{-1}\mathbf{T}_0)\right] \right\}^{K+1}, \tag{9}$$

where

$$\mathbf{T}_0 = \frac{1}{K+1}\left(\mathbf{x}\mathbf{x}^\dagger + \tilde{\mathbf{R}}_p \right). \tag{10}$$

Using the persymmetry structure in the covariance matrix $\mathbf{R}_p$, we have

$$\begin{aligned} \mathrm{tr}(\mathbf{R}_p^{-1}\mathbf{T}_j) &= \mathrm{tr}[\mathbf{J}(\mathbf{R}_\mathbf{p}^*)^{-1}\mathbf{J}\mathbf{T}_j] \\ &= \mathrm{tr}[(\mathbf{R}_\mathbf{p}^*)^{-1}\mathbf{J}\mathbf{T}_j\mathbf{J}] \\ &= \mathrm{tr}[\mathbf{R}_p^{-1}\mathbf{J}\mathbf{T}_j^*\mathbf{J}], \quad j = 0, 1. \end{aligned} \tag{11}$$

As a result, (7) can be rewritten as

$$f_1(\mathbf{x},\mathbf{y}_1,\ldots,\mathbf{y}_K) = \left\{ \frac{1}{\pi^N|\mathbf{R}_p|} \exp\left[-\mathrm{tr}(\mathbf{R}_p^{-1}\mathbf{T}_{1p})\right] \right\}^{K+1}, \tag{12}$$

where

$$\mathbf{T}_{1p} = \frac{1}{2}\left(\mathbf{T}_1 + \mathbf{J}\mathbf{T}_1^*\mathbf{J}\right). \tag{13}$$

As derived in Appendix A, we have

$$\mathbf{T}_{1p} = \frac{1}{K+1}\left[(\mathbf{X}_p - \mathbf{\Sigma}\mathbf{A})(\mathbf{X}_p - \mathbf{\Sigma}\mathbf{A})^\dagger + \hat{\mathbf{R}}_p \right], \tag{14}$$

where

$$\hat{\mathbf{R}}_p = \frac{1}{2}\left(\tilde{\mathbf{R}}_p + \mathbf{J}\tilde{\mathbf{R}}_p^*\mathbf{J} \right) \in \mathbb{C}^{N\times N}, \tag{15}$$

$$\mathbf{X}_p = [\mathbf{x}_e, \mathbf{x}_o] \in \mathbb{C}^{N\times 2}, \tag{16}$$

and

$$\mathbf{A} = [\mathbf{a}_e, \mathbf{a}_o] \in \mathbb{C}^{q\times 2}, \tag{17}$$

with

$$\begin{cases} \mathbf{x}_e = \frac{1}{2}(\mathbf{x} + \mathbf{J}\mathbf{x}^*) \in \mathbb{C}^{N\times 1}, \\ \mathbf{x}_o = \frac{1}{2}(\mathbf{x} - \mathbf{J}\mathbf{x}^*) \in \mathbb{C}^{N\times 1}, \end{cases} \tag{18}$$

and

$$\begin{cases} \mathbf{a}_e = \frac{1}{2}(\mathbf{a} + \mathbf{a}^*) = \mathfrak{Re}(\mathbf{a}), \\ \mathbf{a}_o = \frac{1}{2}(\mathbf{a} - \mathbf{a}^*) = \jmath\,\mathfrak{Im}(\mathbf{a}). \end{cases} \tag{19}$$

Similarly,

$$f_0(\mathbf{x},\mathbf{y}_1,\ldots,\mathbf{y}_K) = \left\{ \frac{1}{\pi^N|\mathbf{R}_p|} \exp\left[-\mathrm{tr}(\mathbf{R}_p^{-1}\mathbf{T}_{0p})\right] \right\}^{K+1}, \tag{20}$$

where

$$\mathbf{T}_{0p} = \frac{1}{K+1}\left(\mathbf{X}_p\mathbf{X}_p^\dagger + \hat{\mathbf{R}}_p \right). \tag{21}$$

It is easy to check that

$$\begin{cases} \max_{\{\mathbf{R}_p\}} f_1(\mathbf{x},\mathbf{y}_1,\ldots,\mathbf{y}_K) = \left[(e\pi)^N|\mathbf{T}_{1p}|\right]^{-(K+1)}, \\ \max_{\{\mathbf{R}_p\}} f_0(\mathbf{x},\mathbf{y}_1,\ldots,\mathbf{y}_K) = \left[(e\pi)^N|\mathbf{T}_{0p}|\right]^{-(K+1)}. \end{cases} \tag{22}$$

As a result, the GLRT in (6) can be equivalently written as

$$\Lambda_2 = \frac{|\mathbf{T}_{0p}|}{\min_{\{\mathbf{A}\}}|\mathbf{T}_{1p}|} \underset{H_0}{\overset{H_1}{\gtrless}} \lambda_2, \tag{23}$$

where λ_2 is a detection threshold. The minimization of $|\mathbf{T}_{1p}|$ with respect to $\mathbf{A}$ can be achieved at

$$\hat{\mathbf{A}} = \left(\boldsymbol{\Sigma}^\dagger \hat{\mathbf{R}}_p^{-1} \boldsymbol{\Sigma}\right)^{-1} \boldsymbol{\Sigma}^\dagger \hat{\mathbf{R}}_p^{-1} \mathbf{X}_p. \tag{24}$$

Hence, we have

$$\min_{\{\mathbf{A}\}} |\mathbf{T}_{1p}| = \frac{1}{(K+1)^N} |\hat{\mathbf{R}}_p| \left|\mathbf{I}_2 + \mathbf{X}_p^\dagger \mathbf{P}_p \mathbf{X}_p\right|, \tag{25}$$

where

$$\mathbf{P}_p = \hat{\mathbf{R}}_p^{-1} - \hat{\mathbf{R}}_p^{-1} \boldsymbol{\Sigma} \left(\boldsymbol{\Sigma}^\dagger \hat{\mathbf{R}}_p^{-1} \boldsymbol{\Sigma}\right)^{-1} \boldsymbol{\Sigma}^\dagger \hat{\mathbf{R}}_p^{-1} \in \mathbb{C}^{N\times N}. \tag{26}$$

It is obvious from (10) that

$$|\mathbf{T}_{0p}| = \frac{1}{(K+1)^N} |\hat{\mathbf{R}}_p| \left|\mathbf{I}_2 + \mathbf{X}_p^\dagger \hat{\mathbf{R}}_p^{-1} \mathbf{X}_p\right|. \tag{27}$$

Substituting (25) and (27) into (23), we derive the one-step persymmetric GLRT detector as

$$\Lambda = \frac{\left|\mathbf{I}_2 + \mathbf{X}_p^\dagger \hat{\mathbf{R}}_p^{-1} \mathbf{X}_p\right|}{\left|\mathbf{I}_2 + \mathbf{X}_p^\dagger \mathbf{P}_p \mathbf{X}_p\right|} \underset{H_0}{\overset{H_1}{\gtrless}} \lambda, \tag{28}$$

where λ is a detection threshold. This detector is referred to as one-step persymmetric GLRT (PGLRT) detector.

IV. Threshold Setting

To complete the construction of the detection scheme in (28), we should provide a way to set the detection threshold λ for a given probability of false alarm. To this end, we derive a finite-sum expression for the probability of false alarm in the following. At the end of this section, we will provide some discussions on the detection probability.

A. Transformation From Complex Domain to Real Domain

For convenience of statistical analysis, we first transform all quantities in the original data from the complex-valued domain to the real-valued domain. Let us start by defining a unitary matrix as

$$\mathbf{D} = \frac{1}{2}\left[(\mathbf{I}_N + \mathbf{J}) + \jmath\,(\mathbf{I}_N - \mathbf{J})\right] \in \mathbb{C}^{N\times N}. \tag{29}$$

Using (16), (18) and (29), we have

$$\mathbf{D}\mathbf{X}_p = [\mathbf{x}_{er}, \jmath\,\mathbf{x}_{or}], \tag{30}$$

where

$$\mathbf{x}_{er} = \mathbf{D}\mathbf{x}_e = \frac{1}{2}\left[(\mathbf{I}_N + \mathbf{J})\mathfrak{Re}(\mathbf{x}) - (\mathbf{I}_N - \mathbf{J})\mathfrak{Im}(\mathbf{x})\right] \in \mathbb{R}^{N\times 1}, \tag{31}$$

and

$$\begin{aligned}\mathbf{x}_{or} &= -\jmath\mathbf{D}\mathbf{x}_o \\ &= \frac{1}{2}\left[(\mathbf{I}_N - \mathbf{J})\mathfrak{Re}(\mathbf{x}) + (\mathbf{I}_N + \mathbf{J})\mathfrak{Im}(\mathbf{x})\right] \in \mathbb{R}^{N\times 1}.\end{aligned} \tag{32}$$

It is worth noting that $\mathbf{x}_{er}$ and $\mathbf{x}_{or}$ are now real-valued column vectors of dimension N.

We proceed by defining another unitary matrix as

$$\mathbf{V}_2 = \begin{bmatrix} 1 & 0 \\ 0 & -\jmath \end{bmatrix} \in \mathbb{C}^{2\times 2}. \tag{33}$$

Now we use the two unitary matrices $\mathbf{D}$ and $\mathbf{V}_2$ to transform all complex-valued quantities in (28) to be real-valued ones. Specifically, we define

$$\mathbf{M} \triangleq \mathbf{D}\hat{\mathbf{R}}_p\mathbf{D}^\dagger = \mathfrak{Re}(\hat{\mathbf{R}}_p) + \mathbf{J}\mathfrak{Im}(\hat{\mathbf{R}}_p) \in \mathbb{R}^{N\times N}, \tag{34}$$

$$\boldsymbol{\Omega} \triangleq \mathbf{D}\boldsymbol{\Sigma} = \mathfrak{Re}(\boldsymbol{\Sigma}) - \mathfrak{Im}(\boldsymbol{\Sigma}) \in \mathbb{R}^{N\times q}, \tag{35}$$

$$\mathbf{X} \triangleq \mathbf{D}\mathbf{X}_p\mathbf{V}_2 = [\mathbf{x}_{er}, \mathbf{x}_{or}] \in \mathbb{R}^{N\times 2}. \tag{36}$$

Then, the proposed one-step PGLRT detector in (28) can be recast to

$$\begin{aligned}\Lambda &= \frac{\left|\mathbf{I}_2 + \mathbf{V}_2\mathbf{X}^\dagger\mathbf{M}^{-1}\mathbf{X}\mathbf{V}_2^\dagger\right|}{\left|\mathbf{I}_2 + \mathbf{V}_2\mathbf{X}^\dagger\mathbf{P}\mathbf{X}\mathbf{V}_2^\dagger\right|} \\ &= \frac{\left|\mathbf{I}_2 + \mathbf{X}^T\mathbf{M}^{-1}\mathbf{X}\right|}{\left|\mathbf{I}_2 + \mathbf{X}^T\mathbf{P}\mathbf{X}\right|} \underset{H_0}{\overset{H_1}{\gtrless}} \lambda,\end{aligned} \tag{37}$$

where

$$\begin{aligned}\mathbf{P} &\triangleq \mathbf{D}\mathbf{P}_p\mathbf{D}^\dagger \\ &= \mathbf{M}^{-1} - \mathbf{M}^{-1}\boldsymbol{\Omega}\left(\boldsymbol{\Omega}^T\mathbf{M}^{-1}\boldsymbol{\Omega}\right)^{-1}\boldsymbol{\Omega}^T\mathbf{M}^{-1} \in \mathbb{R}^{N\times N}.\end{aligned} \tag{38}$$

It is worth pointing out that all quantities in (37) are real-valued. Next, we will perform statistical analysis on the proposed one-step PGLRT detector in the real-valued domain.

B. Statistical Characterizations

First, the statistical properties of $\mathbf{M}$ and $\mathbf{X}$ are provided. As derived in Appendix B, we have

$$\begin{cases}\mathbf{M} \sim \mathcal{W}_N(2K, \mathbf{R}), \\ \mathbf{X} \sim \mathcal{N}(\mathbf{0}, \mathbf{R} \otimes \mathbf{I}_2),\end{cases} \tag{39}$$

where $\mathbf{R}$ is defined in (B.7).

1) Equivalent Form of $\mathbf{X}^T\mathbf{P}\mathbf{X}$: Now we turn to obtain an equivalent form of $\mathbf{X}^T\mathbf{P}\mathbf{X}$. To this end, we define

$$\mathbf{E} \triangleq \boldsymbol{\Omega}(\boldsymbol{\Omega}^T\boldsymbol{\Omega})^{-1/2} \in \mathbb{R}^{N\times q}, \tag{40}$$

and hence

$$\mathbf{E}^T\mathbf{E} = \mathbf{I}_q. \tag{41}$$

Therefore, we can construct an $N \times (N-q)$ matrix $\mathbf{F}$ such that

$$\begin{cases}\mathbf{F}^T\mathbf{E} = \mathbf{0}_{(N-q)\times q}, \\ \mathbf{F}^T\mathbf{F} = \mathbf{I}_{N-q}.\end{cases} \tag{42}$$

Define

$$\mathbf{U} \triangleq [\mathbf{E}, \mathbf{F}] \in \mathbb{R}^{N\times N}. \tag{43}$$

Obviously, $\mathbf{U}$ is an orthogonal matrix, i.e., $\mathbf{U}\mathbf{U}^T = \mathbf{U}^T\mathbf{U} = \mathbf{I}_N$.

Define

$$\begin{cases}\mathbf{X}_1 \triangleq \mathbf{E}^T\mathbf{X} \in \mathbb{R}^{q\times 2}, \\ \mathbf{X}_2 \triangleq \mathbf{F}^T\mathbf{X} \in \mathbb{R}^{(N-q)\times 2},\end{cases} \tag{44}$$

and then we have

$$\begin{bmatrix}\mathbf{X}_1 \\ \mathbf{X}_2\end{bmatrix} = \mathbf{U}^T\mathbf{X}, \tag{45}$$

and

$$\mathbf{X} = \mathbf{E}\mathbf{X}_1 + \mathbf{F}\mathbf{X}_2. \tag{46}$$

Using (38) and the definition of $\mathbf{E}$ in (40), we obtain

$$\begin{cases} \mathbf{P}\mathbf{E} = \mathbf{0}_{N\times q}, \\ \mathbf{E}^T\mathbf{P} = \mathbf{0}_{q\times N}, \end{cases} \tag{47}$$

and

$$\mathbf{P} = \mathbf{M}^{-1} - \mathbf{M}^{-1}\mathbf{E}\left(\mathbf{E}^T\mathbf{M}^{-1}\mathbf{E}\right)^{-1}\mathbf{E}^T\mathbf{M}^{-1}. \tag{48}$$

Employing (46) and (47), we have

$$\mathbf{X}^T\mathbf{P}\mathbf{X} = \mathbf{X}_2^T\mathbf{F}^T\mathbf{P}\mathbf{F}\mathbf{X}_2. \tag{49}$$

In the following, we make an transformation for the term $\mathbf{F}^T\mathbf{P}\mathbf{F}$. Write

$$\mathbf{U}^T\mathbf{M}\mathbf{U} = \begin{bmatrix} \mathbf{M}_{11} & \mathbf{M}_{12} \\ \mathbf{M}_{21} & \mathbf{M}_{22} \end{bmatrix}, \tag{50}$$

where $\mathbf{M}_{11} \in \mathbb{R}^{q\times q}$, $\mathbf{M}_{12} \in \mathbb{R}^{q\times(N-q)}$, $\mathbf{M}_{21} \in \mathbb{R}^{(N-q)\times q}$, and $\mathbf{M}_{22} \in \mathbb{R}^{(N-q)\times(N-q)}$. We note that

$$\begin{aligned} \mathbf{U}^T\mathbf{M}^{-1}\mathbf{U} &= (\mathbf{U}^T\mathbf{M}\mathbf{U})^{-1} \\ &\triangleq \begin{bmatrix} \bar{\mathbf{M}}_{11} & \bar{\mathbf{M}}_{12} \\ \bar{\mathbf{M}}_{21} & \bar{\mathbf{M}}_{22} \end{bmatrix}, \end{aligned} \tag{51}$$

where $\bar{\mathbf{M}}_{11} \in \mathbb{R}^{q\times q}$, $\bar{\mathbf{M}}_{12} \in \mathbb{R}^{q\times(N-q)}$, $\bar{\mathbf{M}}_{21} \in \mathbb{R}^{(N-q)\times q}$, and $\bar{\mathbf{M}}_{22} \in \mathbb{R}^{(N-q)\times(N-q)}$. According to the matrix inversion lemma [45, p. 99, Theorem 8.5.11], we obtain

$$\mathbf{M}_{22}^{-1} = \bar{\mathbf{M}}_{22} - \bar{\mathbf{M}}_{21}\bar{\mathbf{M}}_{11}^{-1}\bar{\mathbf{M}}_{12}. \tag{52}$$

Using (43), we have

$$\mathbf{U}^T\mathbf{M}^{-1}\mathbf{U} = \begin{bmatrix} \mathbf{E}^T\mathbf{M}^{-1}\mathbf{E} & \mathbf{E}^T\mathbf{M}^{-1}\mathbf{F} \\ \mathbf{F}^T\mathbf{M}^{-1}\mathbf{E} & \mathbf{F}^T\mathbf{M}^{-1}\mathbf{F} \end{bmatrix}. \tag{53}$$

Combining (51) and (53), we obtain

$$\begin{bmatrix} \bar{\mathbf{M}}_{11} & \bar{\mathbf{M}}_{12} \\ \bar{\mathbf{M}}_{21} & \bar{\mathbf{M}}_{22} \end{bmatrix} = \begin{bmatrix} \mathbf{E}^T\mathbf{M}^{-1}\mathbf{E} & \mathbf{E}^T\mathbf{M}^{-1}\mathbf{F} \\ \mathbf{F}^T\mathbf{M}^{-1}\mathbf{E} & \mathbf{F}^T\mathbf{M}^{-1}\mathbf{F} \end{bmatrix}. \tag{54}$$

Using (48), we have

$$\begin{aligned} \mathbf{F}^T\mathbf{P}\mathbf{F} &= \mathbf{F}^T\mathbf{M}^{-1}\mathbf{F} - \mathbf{F}^T\mathbf{M}^{-1}\mathbf{E}\left(\mathbf{E}^T\mathbf{M}^{-1}\mathbf{E}\right)^{-1}\mathbf{E}^T\mathbf{M}^{-1}\mathbf{F} \\ &= \bar{\mathbf{M}}_{22} - \bar{\mathbf{M}}_{21}\bar{\mathbf{M}}_{11}^{-1}\bar{\mathbf{M}}_{12} \\ &= \mathbf{M}_{22}^{-1}, \end{aligned} \tag{55}$$

where the second and third lines are obtained from (54) and (52), respectively. Substituting (55) into (49) results in

$$\mathbf{X}^T\mathbf{P}\mathbf{X} = \mathbf{X}_2^T\mathbf{M}_{22}^{-1}\mathbf{X}_2, \tag{56}$$

which is only relative to the 2-components of the data.

2) Equivalent Form of $\mathbf{X}^T\mathbf{M}^{-1}\mathbf{X}$*:* Now we turn our attention to $\mathbf{X}^T\mathbf{M}^{-1}\mathbf{X}$, which can be written as

$$\begin{aligned} \mathbf{X}^T\mathbf{M}^{-1}\mathbf{X} &= (\mathbf{U}^T\mathbf{X})^T(\mathbf{U}^T\mathbf{M}^{-1}\mathbf{U})\mathbf{U}^T\mathbf{X} \\ &= \left[\mathbf{X}_1^T, \mathbf{X}_2^T\right]\begin{bmatrix} \bar{\mathbf{M}}_{11} & \bar{\mathbf{M}}_{12} \\ \bar{\mathbf{M}}_{21} & \bar{\mathbf{M}}_{22} \end{bmatrix}\begin{bmatrix} \mathbf{X}_1 \\ \mathbf{X}_2 \end{bmatrix} \\ &= \mathbf{Z}^T\bar{\mathbf{M}}_{11}\mathbf{Z} + \mathbf{X}_2^T\mathbf{M}_{22}^{-1}\mathbf{X}_2, \end{aligned} \tag{57}$$

where the second and third lines are obtained using (45) and [46, p. 135, eq. (A1-9)], respectively, and

$$\mathbf{Z} \triangleq \mathbf{X}_1 - \mathbf{M}_{12}\mathbf{M}_{22}^{-1}\mathbf{X}_2 \in \mathbb{R}^{q\times 2}. \tag{58}$$

3) Statistical Distribution of Λ*:* Taking (56) and (57) into (37) produces

$$\begin{aligned} \Lambda &= \frac{|\boldsymbol{\Delta} + \mathbf{Z}^T\bar{\mathbf{M}}_{11}\mathbf{Z}|}{|\boldsymbol{\Delta}|} \\ &= |\mathbf{I}_2 + \mathbf{G}^T\bar{\mathbf{M}}_{11}\mathbf{G}| \underset{H_0}{\overset{H_1}{\gtrless}} \lambda, \end{aligned} \tag{59}$$

where

$$\boldsymbol{\Delta} \triangleq \mathbf{I}_2 + \mathbf{X}_2^T\mathbf{M}_{22}^{-1}\mathbf{X}_2 \in \mathbb{R}^{2\times 2}, \tag{60}$$

and

$$\mathbf{G} \triangleq \mathbf{Z}\Delta^{-1/2} \in \mathbb{R}^{q\times 2}. \tag{61}$$

Now we can rewrite (59) as

$$\Lambda = \frac{|\bar{\mathbf{M}}_{11} + \mathbf{G}\mathbf{G}^T|}{|\bar{\mathbf{M}}_{11}|} \underset{H_0}{\overset{H_1}{\gtrless}} \lambda, \tag{62}$$

where $\bar{\mathbf{M}}_{11}$ and $\mathbf{G}$ are independent, and their distributions under H_0 are given by (see the detailed derivations in Appendix C)

$$\begin{cases} \bar{\mathbf{M}}_{11} \sim \mathcal{W}_q(2K - N + q, \bar{\mathbf{R}}_{11}^{-1}), \\ \mathbf{G} \sim \mathcal{N}(\mathbf{0}, \bar{\mathbf{R}}_{11}^{-1} \otimes \mathbf{I}_2), \end{cases} \tag{63}$$

with $\bar{\mathbf{R}}_{11}$ defined in (C.4). According to [47, p. 305, Lemma 8.4.2], Λ^{-1} under H_0 has the central Wilks' Lambda distribution, written as

$$\Lambda^{-1} \sim U_{q,\,2,\,2K+q-N}, \tag{64}$$

where $U_{n,m,j}$ denotes the central Wilks' Lambda distribution with n, m and j being the number of dimensions, the hypothesis degrees of freedom, and the error degrees of freedom, respectively.

C. Probability of False Alarm

According to [47, p. 311, Theorem 8.4.6], we have

$$\frac{1 - \sqrt{\Lambda^{-1}}}{\sqrt{\Lambda^{-1}}} \sim \frac{q}{2K - N + 1} F_{2q,\,2(2K-N+1)}. \tag{65}$$

As a result,

$$\sqrt{\Lambda} - 1 \sim \frac{\chi_{2q}^2}{\chi_{2(2K-N+1)}^2}. \tag{66}$$

Now we can equivalently write (62) as

$$\frac{t}{\tau} \underset{H_0}{\overset{H_1}{\gtrless}} \sqrt{\lambda} - 1, \tag{67}$$

where t and τ are independent real-valued random variables. Under H_0, these two random variables are distributed as

$$\begin{cases} t \sim \frac{1}{2}\chi_{2q}^2, \\ \tau \sim \frac{1}{2}\chi_{2(2K-N+1)}^2. \end{cases} \tag{68}$$

Similar to the derivation of the probability of false alarm in [17], we can obtain an analytical expression for the probability of false alarm as

$$P_{\text{FA}} = \sum_{j=1}^{q} \mathrm{C}_{2K+q-N-j}^{q-j} \left(\sqrt{\lambda} - 1\right)^{q-j} \lambda^{-\frac{2K+q+1-N-j}{2}}. \tag{69}$$

It can be seen that the proposed one-step PGLRT detector exhibits the CFAR property against the clutter covariance matrix, since (69) is independent of the clutter covariance matrix.

As to the detection probability of the proposed one-step PGLRT detector, we cannot obtain an analytical expression for it. This is because that the test statistic Λ under H_1 is subject to a noncentral Wilks' Lambda distribution whose complementary cumulative distribution function is quite complicated [48], if not intractable.

V. Numerical Examples

In this section, numerical simulations are provided to verify the above theoretical results. Assume that a pulsed Doppler radar is used, which transmits symmetrically spaced pulse trains. The number of pulses in a coherent processing interval is $N = 8$. The (i, j)th element of the clutter covariance matrix is chosen as $[\mathbf{R}]_{i,j} = \sigma^2 0.9^{|i-j|}$, where σ^2 is the clutter power. The target coordinate vector is $\mathbf{a} = \sigma_a[1, 1, \ldots, 1]^T$, where σ_a^2 is the target power. The signal-to-clutter ratio (SCR) in decibel is defined by $\mathrm{SCR} = 10\log_{10}\frac{\sigma_a^2}{\sigma^2}$. The target subspace matrix $\mathbf{\Sigma}$ is chosen to be

$$\mathbf{\Sigma} = [\mathbf{p}(f_{\mathrm{d},1}), \mathbf{p}(f_{\mathrm{d},2}), \ldots, \mathbf{p}(f_{\mathrm{d},q})], \tag{70}$$

where $f_{\mathrm{d},i}$ is the i-th normalized Doppler frequency, and for $i = 1, 2, \ldots, q$,

$$\mathbf{p}(f_{\mathrm{d},i}) = \frac{1}{\sqrt{N}}\left[\mathrm{e}^{-\jmath 2\pi f_{\mathrm{d},i}\frac{(N-1)}{2}}, \ldots, \mathrm{e}^{-\jmath 2\pi f_{\mathrm{d},i}\frac{1}{2}}, \mathrm{e}^{\jmath 2\pi f_{\mathrm{d},i}\frac{1}{2}}, \ldots, \mathrm{e}^{\jmath 2\pi f_{\mathrm{d},i}\frac{(N-1)}{2}}\right]^T, \tag{71}$$

for even N, and

$$\mathbf{p}(f_{\mathrm{d},i}) = \frac{1}{\sqrt{N}}\left[\mathrm{e}^{-\jmath 2\pi f_{\mathrm{d},i}\frac{(N-1)}{2}}, \ldots, \mathrm{e}^{-\jmath 2\pi f_{\mathrm{d},i}}, 1, \mathrm{e}^{\jmath 2\pi f_{\mathrm{d},i}}, \ldots, \mathrm{e}^{\jmath 2\pi f_{\mathrm{d},i}\frac{(N-1)}{2}}\right]^T, \tag{72}$$

for odd N. For comparison purposes, the conventional PAMF [38, eq. (14)], and Cai-Wang's GLRT [34, eq. (13)] are considered. Note that all these conventional adaptive detectors bear the CFAR property against the clutter covariance matrix.

In Fig. 1, the probability of false alarm as a function of the threshold λ is presented for two cases: $q = 2$ and $q = 3$. For $q = 2$, we select $f_{\mathrm{d},1} = 0.07$ and $f_{\mathrm{d},2} = 0.1$, while for $q = 3$, we choose $f_{\mathrm{d},1} = 0.07$, $f_{\mathrm{d},2} = 0.1$ and $f_{\mathrm{d},3} = 0.13$. The symbols denote MC results, while the lines denote the theoretical results using (69). As shown, the theoretical results are consistent with the MC ones.

In the following simulations, the normalized Doppler frequency in the nominal target steering vector (denoted by $\mathbf{p}_t$) is chosen to be 0.1, i.e., $\mathbf{p}_t = \mathbf{p}(0.1)$. As suggested in [43], we combine the nominal steering vector and its adjacent ones to span the signal subspace. Specifically, we select $q = 3$, $f_{\mathrm{d},1} = 0.07$, $f_{\mathrm{d},2} = 0.1$ and $f_{\mathrm{d},3} = 0.13$. Note that the true nominal target steering vector (denoted by $\tilde{\mathbf{p}}_t$) may not be aligned with the nominal one. The mismatch between the nominal and true target steering vectors is defined as

$$\cos^2\phi = \frac{|\mathbf{p}_t^\dagger \mathbf{R}^{-1}\tilde{\mathbf{p}}_t|^2}{(\mathbf{p}_t^\dagger \mathbf{R}^{-1}\mathbf{p}_t)(\tilde{\mathbf{p}}_t^\dagger \mathbf{R}^{-1}\tilde{\mathbf{p}}_t)}. \tag{73}$$

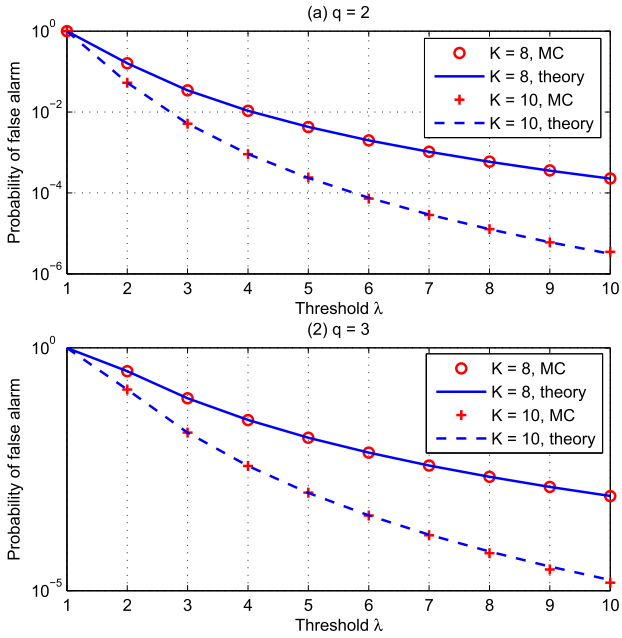

Fig. 1. Probability of false alarm versus threshold. The line denotes the results computed with the finite-sum expression (69), and the symbol stands for the MC result.

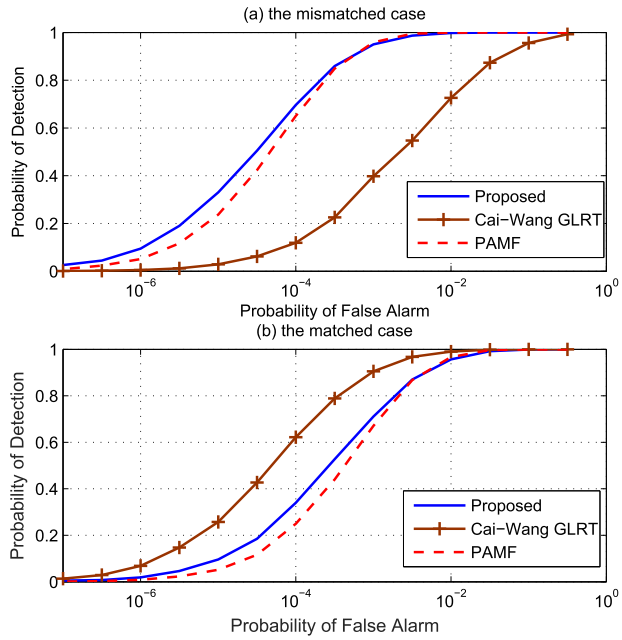

Fig. 2. Receiver operating characteristic curves for $K = N = 8$, $q = 3$, and SCR = 15 dB. (a) The mismatched case: $\cos^2\phi = 0.7436$; (b) The matched case: $\cos^2\phi = 1$.

In Fig. 2, we plot the receiver operating characteristic (ROC) curves for $N = K = 8$ and SCR = 15 dB. Due to the lack of analytical expression for the detection probability, we resort to MC techniques to simulate the detection probability. We consider the matched case with $\cos^2\phi = 1$, and the mismatched case with $\cos^2\phi = 0.7436$ (the corresponding normalized Doppler frequency of the target is 0.14).

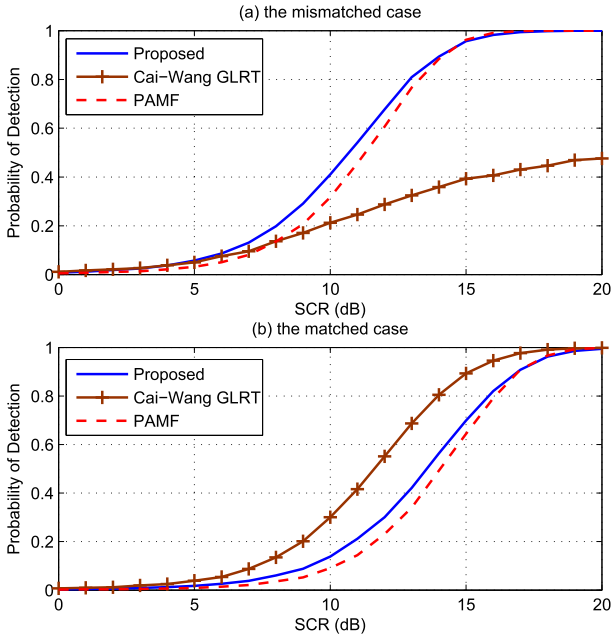

Fig. 3. Detection probability versus SCR for $K = N = 8$, $q = 3$ and $P_{\text{FA}} = 10^{-3}$. (a) The mismatched case: $\cos^2\phi = 0.7436$; (b) The matched case: $\cos^2\phi = 1$.

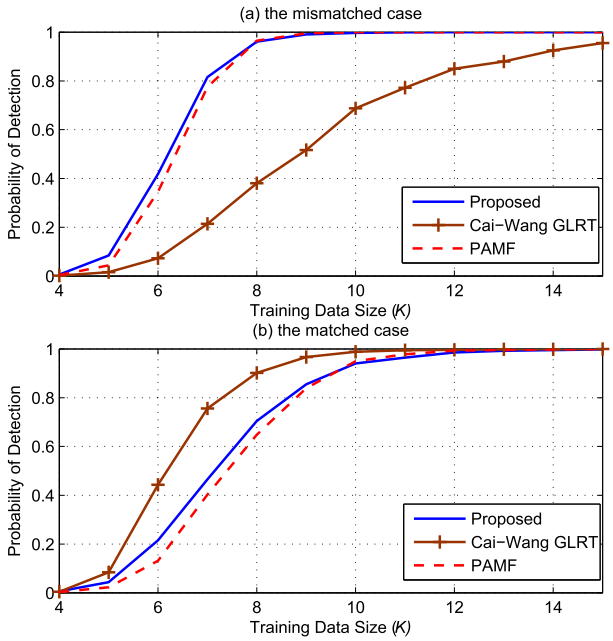

Fig. 4. Detection probability versus K for $N = 8$, $q = 3$, SCR = 15 dB and $P_{\text{FA}} = 10^{-3}$. (a) The mismatched case: $\cos^2\phi = 0.7436$; (b) The matched case: $\cos^2\phi = 1$.

It can be observed in Fig. 2 that the proposed detector and the PAMF perform much better than the Cai-Wang's GLRT detector in the mismatched case. This is because a subspace model is exploited to improve robustness. Nevertheless, the proposed detector and the PAMF have worse performance than the Cai-Wang's GLRT detector in the matched case. Their performance loss in the matched case can be explained as the cost to achieve improved robustness in the mismatched case. Another interesting phenomenon is observed: our proposed detector outperforms the PAMF detector, only when the probability of false alarm is low (e.g., $P_{\text{FA}} \leq 10^{-4}$). It means that our proposed detector does not always outperform the PAMF. This is as expected. In fact, no uniformly most powerful invariant test exists for the detection problem considered [5].

Fig. 3 plots the detection probability versus the SCR for $K = N = 8$. The probability of false alarm is selected to be 10^{-3}. We can observe that the proposed detector and the PAMF detector have strong robustness in the mismatched case, but perform worse than Cai-Wang's GLRT detector in the matched case. In addition, the proposed detector outperforms the PAMF detector in the region of low or moderate SCRs. When the SCR is high, the PAMF has slightly better performance than the proposed detector. These phenomena are consistent with those in [22] and [9].

In Fig. 4, we depict the detection probability as a function of K, where SCR = 15 dB and the probability of false alarm is 10^{-3}. It can be seen that compared with Cai-Wang's GLRT detector, the proposed detector is more robust to the target steering vector mismatch, but has a performance loss in the matched case. In addition, our proposed detector outperforms the PAMF detector, when the training data size is small or moderate.

VI. Conclusions

The subspace signal detection problem has been considered in homogeneous Gaussian clutter with unknown covariance matrix. By exploiting persymmetry, we proposed the one-step PGLRT detector according to the one-step method. We derived an exact expression for the probability of false alarm, which can facilitate the threshold setting. It is indicated that the proposed one-step PGLRT detector has the CFAR property with respect to the clutter covariance matrix. Numerical examples show that compared to Cai-Wang's GLRT in [34], our proposed one-step PGLRT detector is more robust to the target steering vector mismatch, but suffers from performance loss in the matched case. It is also shown in the simulations that our proposed detector slightly outperforms the PAMF detector in some cases (e.g., low probability of false alarm, low SNRs, or low training data size).

Appendix A
Derivations of (14)

Define

$$\begin{cases} \tilde{\mathbf{T}}_1 = (\mathbf{x} - \boldsymbol{\Sigma}\mathbf{a})(\mathbf{x} - \boldsymbol{\Sigma}\mathbf{a})^\dagger + \tilde{\mathbf{R}}_p, \\ \tilde{\mathbf{T}}_{1p} = (\mathbf{X}_p - \boldsymbol{\Sigma}\mathbf{A})(\mathbf{X}_p - \boldsymbol{\Sigma}\mathbf{A})^\dagger + \hat{\mathbf{R}}_p. \end{cases} \tag{A.1}$$

Then, (14) holds true if the following equation is valid:

$$\tilde{\mathbf{T}}_{1p} = \frac{1}{2}\left(\tilde{\mathbf{T}}_1 + \mathbf{J}\tilde{\mathbf{T}}_1^*\mathbf{J}\right), \tag{A.2}$$

which is derived as follows. Using (A.1), we have

$$\tilde{\mathbf{T}}_1 + \mathbf{J}\tilde{\mathbf{T}}_1^*\mathbf{J} = \tilde{\mathbf{R}}_p + \mathbf{J}\tilde{\mathbf{R}}_p^*\mathbf{J} + \mathbf{H}, \tag{A.3}$$

where

$$\begin{aligned}\mathbf{H} &= (\mathbf{x}-\boldsymbol{\Sigma}\mathbf{a})(\mathbf{x}-\boldsymbol{\Sigma}\mathbf{a})^{\dagger} + \mathbf{J}(\mathbf{x}-\boldsymbol{\Sigma}\mathbf{a})^{*}(\mathbf{x}-\boldsymbol{\Sigma}\mathbf{a})^{T}\mathbf{J} \\ &= \mathbf{x}\mathbf{x}^{\dagger} + \mathbf{J}\mathbf{x}^{*}\mathbf{x}^{T}\mathbf{J} - \left(\mathbf{x}\mathbf{a}^{\dagger}\boldsymbol{\Sigma}^{\dagger} + \mathbf{J}\mathbf{x}^{*}\mathbf{a}^{T}\boldsymbol{\Sigma}^{T}\mathbf{J}\right) \\ &\quad - \left(\boldsymbol{\Sigma}\mathbf{a}\mathbf{x}^{\dagger} + \mathbf{J}\boldsymbol{\Sigma}^{*}\mathbf{a}^{*}\mathbf{x}^{T}\mathbf{J}\right) \\ &\quad + \left(\boldsymbol{\Sigma}\mathbf{a}\mathbf{a}^{\dagger}\boldsymbol{\Sigma}^{\dagger} + \mathbf{J}\boldsymbol{\Sigma}^{*}\mathbf{a}^{*}\mathbf{a}^{T}\boldsymbol{\Sigma}^{T}\mathbf{J}\right).\end{aligned} \tag{A.4}$$

It is easy to check that

$$\begin{cases} 2\mathbf{X}_p\mathbf{X}_p^{\dagger} = \mathbf{x}\mathbf{x}^{\dagger} + \mathbf{J}\mathbf{x}^{*}\mathbf{x}^{T}\mathbf{J}, \\ 2\boldsymbol{\Sigma}\mathbf{A}\mathbf{A}^{\dagger}\boldsymbol{\Sigma}^{\dagger} = \boldsymbol{\Sigma}\mathbf{a}\mathbf{a}^{\dagger}\boldsymbol{\Sigma}^{\dagger} + \mathbf{J}\boldsymbol{\Sigma}^{*}\mathbf{a}^{*}\mathbf{a}^{T}\boldsymbol{\Sigma}^{T}\mathbf{J}, \end{cases} \tag{A.5}$$

and

$$\begin{cases} 2\mathbf{X}_p\mathbf{A}^{\dagger}\boldsymbol{\Sigma}^{\dagger} = \mathbf{x}\mathbf{a}^{\dagger}\boldsymbol{\Sigma}^{\dagger} + \mathbf{J}\mathbf{x}^{*}\mathbf{a}^{T}\boldsymbol{\Sigma}^{T}\mathbf{J}, \\ 2\boldsymbol{\Sigma}\mathbf{A}\mathbf{X}_p^{\dagger} = \boldsymbol{\Sigma}\mathbf{a}\mathbf{x}^{\dagger} + \mathbf{J}\boldsymbol{\Sigma}^{*}\mathbf{a}^{*}\mathbf{x}^{T}\mathbf{J}, \end{cases} \tag{A.6}$$

where $\boldsymbol{\Sigma}^{\dagger} = \boldsymbol{\Sigma}^{T}\mathbf{J}$ is used. Taking (A.5) and (A.6) into (A.4) produces

$$\mathbf{H} = 2\left(\mathbf{X}_p - \boldsymbol{\Sigma}\mathbf{A}\right)\left(\mathbf{X}_p - \boldsymbol{\Sigma}\mathbf{A}\right)^{\dagger}. \tag{A.7}$$

Substituting (A.7) into (A.3), and using (A.1), we obtain (A.2). That is to say, (14) holds true.

Appendix B
Derivations of (39)

Define $\tilde{\mathbf{Y}} = [\mathbf{y}_{e1}, \ldots, \mathbf{y}_{eK}, \mathbf{y}_{o1}, \ldots, \mathbf{y}_{oK}] \in \mathbb{C}^{N\times 2K}$, where

$$\begin{cases} \mathbf{y}_{ek} \triangleq \frac{1}{2}\left(\mathbf{y}_k + \mathbf{J}\mathbf{y}_k^{*}\right), \\ \mathbf{y}_{ok} \triangleq \frac{1}{2}\left(\mathbf{y}_k - \mathbf{J}\mathbf{y}_k^{*}\right). \end{cases} \tag{B.1}$$

Define $\mathbf{Y} \triangleq \mathbf{D}\tilde{\mathbf{Y}}\mathbf{V}_{2K}$, where

$$\mathbf{V}_{2K} = \begin{bmatrix} \mathbf{I}_K & \mathbf{0} \\ \mathbf{0} & -\jmath\mathbf{I}_K \end{bmatrix} \in \mathbb{C}^{2K\times 2K}. \tag{B.2}$$

Then, we have

$$\mathbf{Y} = [\mathbf{y}_{er1}, \ldots, \mathbf{y}_{erK}, \mathbf{y}_{or1}, \ldots, \mathbf{y}_{orK}] \in \mathbb{R}^{N\times 2K}, \tag{B.3}$$

where

$$\begin{aligned}\mathbf{y}_{erk} &\triangleq \mathbf{D}\mathbf{y}_{ek} \\ &= \frac{1}{2}\left[(\mathbf{I}_N + \mathbf{J})\mathfrak{Re}(\mathbf{y}_k) - (\mathbf{I}_N - \mathbf{J})\mathfrak{Im}(\mathbf{y}_k)\right] \in \mathbb{R}^{N\times 1},\end{aligned} \tag{B.4}$$

and

$$\begin{aligned}\mathbf{y}_{ork} &\triangleq -\jmath\mathbf{D}\mathbf{y}_{ok} \\ &= \frac{1}{2}\left[(\mathbf{I}_N - \mathbf{J})\mathfrak{Re}(\mathbf{y}_k) + (\mathbf{I}_N + \mathbf{J})\mathfrak{Im}(\mathbf{y}_k)\right] \in \mathbb{R}^{N\times 1},\end{aligned} \tag{B.5}$$

for $k = 1, 2, \ldots, K$. Moreover,

$$\begin{cases} \mathbf{y}_{erk} \sim \mathcal{N}(\mathbf{0}, \mathbf{R}), \\ \mathbf{y}_{ork} \sim \mathcal{N}(\mathbf{0}, \mathbf{R}), \end{cases} \tag{B.6}$$

where $k = 1, 2, \ldots, K$, they are independent of each other, and

$$\mathbf{R} = \frac{1}{2}\mathbf{D}\mathbf{R}_p\mathbf{D}^{\dagger} = \frac{1}{2}\left[\mathfrak{Re}(\mathbf{R}_p) + \mathbf{J}\mathfrak{Im}(\mathbf{R}_p)\right] \in \mathbb{R}^{N\times N}. \tag{B.7}$$

That is to say, $\mathbf{Y} \sim \mathcal{N}(\mathbf{0}, \mathbf{R}\otimes\mathbf{I}_{2K})$. According to [34, eq. (B11)], we have

$$\mathbf{M} = \mathbf{Y}\mathbf{Y}^{T}. \tag{B.8}$$

Thus,

$$\mathbf{M} \sim \mathcal{W}_N(2K, \mathbf{R}). \tag{B.9}$$

Similar to (B.6), we have

$$\begin{cases} \mathbf{x}_{er} \sim \mathcal{N}(\mathbf{0}, \mathbf{R}), \\ \mathbf{x}_{or} \sim \mathcal{N}(\mathbf{0}, \mathbf{R}). \end{cases} \tag{B.10}$$

It follows from (36) and (B.10) that under H_0,

$$\mathbf{X} \sim \mathcal{N}(\mathbf{0}, \mathbf{R}\otimes\mathbf{I}_2). \tag{B.11}$$

Until now we have derived the distributions of $\mathbf{M}$ and $\mathbf{X}$ as shown in (B.9) and (B.11), respectively. In summary, (39) holds true.

Appendix C
Derivations of (63)

Here we aim to derive the distributions of $\mathbf{G}$ and $\bar{\mathbf{M}}_{11}$. Let us begin by writing

$$\mathbf{U}^{T}\mathbf{R}\mathbf{U} = \begin{bmatrix} \mathbf{R}_{11} & \mathbf{R}_{12} \\ \mathbf{R}_{21} & \mathbf{R}_{22} \end{bmatrix} \tag{C.1}$$

and

$$\mathbf{U}^{T}\mathbf{R}^{-1}\mathbf{U} = \begin{bmatrix} \bar{\mathbf{R}}_{11} & \bar{\mathbf{R}}_{12} \\ \bar{\mathbf{R}}_{21} & \bar{\mathbf{R}}_{22} \end{bmatrix}, \tag{C.2}$$

where $\mathbf{R}_{11} \in \mathbb{R}^{q\times q}$, $\mathbf{R}_{12} \in \mathbb{R}^{q\times(N-q)}$, $\mathbf{R}_{21} \in \mathbb{R}^{(N-q)\times q}$, $\mathbf{R}_{22} \in \mathbb{R}^{(N-q)\times(N-q)}$, $\bar{\mathbf{R}}_{11} \in \mathbb{R}^{q\times q}$, $\bar{\mathbf{R}}_{12} \in \mathbb{R}^{q\times(N-q)}$, $\bar{\mathbf{R}}_{21} \in \mathbb{R}^{(N-q)\times q}$, and $\bar{\mathbf{R}}_{22} \in \mathbb{R}^{(N-q)\times(N-q)}$. It is straightforward to show that

$$\begin{bmatrix} \mathbf{R}_{11} & \mathbf{R}_{12} \\ \mathbf{R}_{21} & \mathbf{R}_{22} \end{bmatrix}^{-1} = \begin{bmatrix} \bar{\mathbf{R}}_{11} & \bar{\mathbf{R}}_{12} \\ \bar{\mathbf{R}}_{21} & \bar{\mathbf{R}}_{22} \end{bmatrix}, \tag{C.3}$$

and

$$\bar{\mathbf{R}}_{11}^{-1} = \mathbf{R}_{11} - \mathbf{R}_{12}\mathbf{R}_{22}^{-1}\mathbf{R}_{21}. \tag{C.4}$$

According to [47, p. 262, Theorem 7.3.6], we have

$$\bar{\mathbf{M}}_{11} \sim \mathcal{W}_q(2K - N + q, \bar{\mathbf{R}}_{11}^{-1}). \tag{C.5}$$

Define

$$\begin{cases} \mathbf{Y}_1 \triangleq \mathbf{E}^{T}\mathbf{Y} \in \mathbb{R}^{q\times 2K}, \\ \mathbf{Y}_2 \triangleq \mathbf{F}^{T}\mathbf{Y} \in \mathbb{R}^{(N-q)\times 2K}, \end{cases} \tag{C.6}$$

and we have

$$\begin{bmatrix} \mathbf{Y}_1 \\ \mathbf{Y}_2 \end{bmatrix} = \mathbf{U}^{T}\mathbf{Y}. \tag{C.7}$$

Then,

$$\mathbf{U}^{T}\mathbf{M}\mathbf{U} = \mathbf{U}^{T}\mathbf{Y}\mathbf{Y}^{T}\mathbf{U} = \begin{bmatrix} \mathbf{Y}_1\mathbf{Y}_1^{T} & \mathbf{Y}_1\mathbf{Y}_2^{T} \\ \mathbf{Y}_2\mathbf{Y}_1^{T} & \mathbf{Y}_2\mathbf{Y}_2^{T} \end{bmatrix}, \tag{C.8}$$

where we have used (B.8) and (C.7). Comparing (50) and (C.8), we can obtain that

$$\mathbf{M}_{12} = \mathbf{Y}_1\mathbf{Y}_2^{T}, \tag{C.9}$$

and

$$\mathbf{M}_{22} = \mathbf{Y}_2\mathbf{Y}_2^{T}. \tag{C.10}$$

Substituting (C.9) into (58) leads to

$$\mathbf{Z} = \mathbf{X}_1 - \mathbf{Y}_1\mathbf{Y}_2^{T}\mathbf{M}_{22}^{-1}\mathbf{X}_2. \tag{C.11}$$

Due to (B.11), the PDF of $\mathbf{X}$ can be written as

$$f(\mathbf{X}) = \frac{1}{(2\pi)^N|\mathbf{R}|}\exp\left[-\frac{1}{2}\text{tr}\left(\mathbf{X}^T\mathbf{R}^{-1}\mathbf{X}\right)\right]. \quad \text{(C.12)}$$

According to [45, p. 188, Theorem 13.3.8], we have

$$\begin{aligned}|\mathbf{R}| &= |\mathbf{R}_{22}||\mathbf{R}_{11}-\mathbf{R}_{12}\mathbf{R}_{22}^{-1}\mathbf{R}_{21}| \\ &= |\mathbf{R}_{22}||\bar{\mathbf{R}}_{11}^{-1}|.\end{aligned} \quad \text{(C.13)}$$

It follows from (45) that

$$\begin{aligned}\mathbf{X}^T\mathbf{R}^{-1}\mathbf{X} &= \left[\mathbf{X}_1^T,\mathbf{X}_2^T\right]\mathbf{U}^T\mathbf{R}^{-1}\mathbf{U}\begin{bmatrix}\mathbf{X}_1\\ \mathbf{X}_2\end{bmatrix} \\ &= \left[\mathbf{X}_1^T,\mathbf{X}_2^T\right]\begin{bmatrix}\bar{\mathbf{R}}_{11} & \bar{\mathbf{R}}_{12}\\ \bar{\mathbf{R}}_{21} & \bar{\mathbf{R}}_{22}\end{bmatrix}\begin{bmatrix}\mathbf{X}_1\\ \mathbf{X}_2\end{bmatrix} \\ &= (\mathbf{X}_1-\bar{\mathbf{X}}_1)^T\bar{\mathbf{R}}_{11}(\mathbf{X}_1-\bar{\mathbf{X}}_1)+\mathbf{X}_2^T\mathbf{R}_{22}^{-1}\mathbf{X}_2,\end{aligned} \quad \text{(C.14)}$$

where the second and third equations are obtained using (C.2) and [46, p. 135, eq. (A1-9)], respectively, and $\bar{\mathbf{X}}_1 = \mathbf{R}_{12}\mathbf{R}_{22}^{-1}\mathbf{X}_2$. Substituting (C.13) and (C.14) into (C.12) yields

$$f(\mathbf{X}) = f(\mathbf{X}_1|\mathbf{X}_2)f(\mathbf{X}_2), \quad \text{(C.15)}$$

where

$$f(\mathbf{X}_1|\mathbf{X}_2) = \frac{\exp\left\{-\frac{1}{2}\text{tr}\left[\bar{\mathbf{R}}_{11}(\mathbf{X}_1-\bar{\mathbf{X}}_1)(\mathbf{X}_1-\bar{\mathbf{X}}_1)^T\right]\right\}}{(2\pi)^q|\bar{\mathbf{R}}_{11}^{-1}|}, \quad \text{(C.16)}$$

and

$$f(\mathbf{X}_2) = \frac{1}{(2\pi)^{N-q}|\mathbf{R}_{22}|}\exp\left[-\frac{1}{2}\text{tr}\left(\mathbf{R}_{22}^{-1}\mathbf{X}_2\mathbf{X}_2^T\right)\right]. \quad \text{(C.17)}$$

We fix temporarily the 2-components of the data. It can be seen from (C.16) that the PDF of $\mathbf{X}_1$ conditioned on $\mathbf{X}_2$ is

$$\mathbf{X}_1 \sim \mathcal{N}(\bar{\mathbf{X}}_1, \bar{\mathbf{R}}_{11}^{-1}\otimes\mathbf{I}_2). \quad \text{(C.18)}$$

That means that the covariance matrix of $\mathbf{X}_1$ conditioned on the 2-components is

$$\text{Cov}_2(\mathbf{X}_1) = \bar{\mathbf{R}}_{11}^{-1}\otimes\mathbf{I}_2, \quad \text{(C.19)}$$

where $\bar{\mathbf{R}}_{11}^{-1}$ is given in (C.4). Similarly, we can derive the covariance matrix of $\mathbf{Y}_1$ conditioned on the 2-components as

$$\text{Cov}_2(\mathbf{Y}_1) = \bar{\mathbf{R}}_{11}^{-1}\otimes\mathbf{I}_{2K}. \quad \text{(C.20)}$$

From (C.11), we can obtain the covariance matrix of $\mathbf{Z}$ conditioned on the 2-components as

$$\begin{aligned}\text{Cov}_2(\mathbf{Z}) &= \text{Cov}_2(\mathbf{X}_1)+\text{Cov}_2(\mathbf{Y}_1)\mathbf{Y}_2^T\mathbf{M}_{22}^{-1}\mathbf{X}_2 \\ &= \bar{\mathbf{R}}_{11}^{-1}\otimes\mathbf{I}_2+\bar{\mathbf{R}}_{11}^{-1}\otimes(\mathbf{X}_2^T\mathbf{M}_{22}^{-1}\mathbf{Y}_2\mathbf{Y}_2^T\mathbf{M}_{22}^{-1}\mathbf{X}_2) \\ &= \bar{\mathbf{R}}_{11}^{-1}\otimes\mathbf{I}_2+\bar{\mathbf{R}}_{11}^{-1}\otimes(\mathbf{X}_2^T\mathbf{M}_{22}^{-1}\mathbf{X}_2) \\ &= \bar{\mathbf{R}}_{11}^{-1}\otimes\boldsymbol{\Delta},\end{aligned} \quad \text{(C.21)}$$

where the third and last lines are obtained using (C.10) and (60), respectively. Using (61) and (C.21), we can obtain that under H_0,

$$\mathbf{G} \sim \mathcal{N}(\mathbf{0}, \bar{\mathbf{R}}_{11}^{-1}\otimes\mathbf{I}_2). \quad \text{(C.22)}$$

Combining (C.5) and (C.22) achieves (63).

REFERENCES

[1] V. Carotenuto, A. De Maio, D. Orlando, and L. Pallotta, "Adaptive radar detection using two sets of training data," *IEEE Trans. Signal Process.*, vol. 66, no. 7, pp. 1791–1801, Apr. 2018.

[2] A. De Maio, "Rao test for adaptive detection in Gaussian interference with unknown covariance matrix," *IEEE Trans. Signal Process.*, vol. 55, no. 7, pp. 3577–3584, Jul. 2007.

[3] P. Wang, H. Li, and B. Himed, "A new parametric GLRT for multichannel adaptive signal detection," *IEEE Trans. Signal Process.*, vol. 58, no. 1, pp. 317–325, Jan. 2010.

[4] A. De Maio, S. Han, and D. Orlando, "Adaptive radar detectors based on the observed FIM," *IEEE Trans. Signal Process.*, vol. 66, no. 14, pp. 3838–3847, Jul. 2018.

[5] S. Bose and A. O. Steinhardt, "A maximal invariant framework for adaptive detection with structured and unstructured covariance matrices," *IEEE Trans. Signal Process.*, vol. 43, no. 9, pp. 2164–2175, Sep. 1995.

[6] W. Liu, J. Liu, Q. Du, and Y. Wang, "Distributed target detection in partially homogeneous environment when signal mismatch occurs," *IEEE Trans. Signal Process.*, vol. 66, no. 14, pp. 3918–3928, Jul. 2018.

[7] P. Wang, H. Li, and B. Himed, "Knowledge-aided parametric tests for multichannel adaptive signal detection," *IEEE Trans. Signal Process.*, vol. 59, no. 12, pp. 5970–5982, Dec. 2011.

[8] E. J. Kelly, "An adaptive detection algorithm," *IEEE Tran. Aerosp. Electron. Syst.*, vol. AES-22, no. 1, pp. 115–127, Mar. 1986.

[9] F. C. Robey, D. R. Fuhrmann, E. J. Kelly, and R. Nitzberg, "A CFAR adaptive matched filter detector," *IEEE Tran. Aerosp. Electron. Syst.*, vol. 28, no. 1, pp. 208–216, Jan. 1992.

[10] F. Bandiera, D. Orlando, and G. Ricci, *Advanced Radar Detection Schemes Under Mismatched Signal Models*. San Rafael, CA, USA: Morgan & Claypool, 2009.

[11] D. Ciuonzo, A. De Maio, and D. Orlando, "On the statistical invariance for adaptive radar detection in partially homogeneous disturbance plus structured interference," *IEEE Trans. Signal Process.*, vol. 5, no. 65, pp. 1222–1234, Mar. 2017.

[12] F. Gini and A. Farina, "Vector subspace detection in compound-Gaussian clutter—Part I: Survey and new results," *IEEE Tran. Aerosp. Electron. Syst.*, vol. 38, no. 4, pp. 1295–1311, Oct. 2002.

[13] J. Liu, W. Liu, B. Chen, H. Liu, H. Li, and C. Hao, "Modified Rao test for multichannel adaptive signal detection," *IEEE Trans. Signal Process.*, vol. 64, no. 3, pp. 714–725, Feb. 2016.

[14] L. L. Scharf and B. Friedlander, "Matched subspace detectors," *IEEE Trans. Signal Process.*, vol. 42, no. 8, pp. 2146–2157, Aug. 1994.

[15] S. Kraut, L. L. Scharf, and L. T. McWhorter, "Adaptive subspace detectors," *IEEE Trans. Signal Process.*, vol. 49, no. 1, pp. 1–16, Jan. 2001.

[16] Y. Jin and B. Friedlander, "A CFAR adaptive subspace detector for second-order Gaussian signals," *IEEE Trans. Signal Process.*, vol. 53, no. 3, pp. 871–884, Mar. 2005.

[17] J. Liu, Z.-J. Zhang, Y. Yang, and H. Liu, "A CFAR adaptive subspace detector for first-order or second-order Gaussian signals based on a single observation," *IEEE Trans. Signal Process.*, vol. 59, no. 11, pp. 5126–5140, Nov. 2011.

[18] W. Liu, W. Xie, J. Liu, and Y. Wang, "Adaptive double subspace signal detection in Gaussian background—Part I: Homogeneous environments," *IEEE Trans. Signal Process.*, vol. 62, no. 9, pp. 2345–2357, May 2014.

[19] W. Liu, W. Xie, J. Liu, and Y. Wang, "Adaptive double subspace signal detection in Gaussian background—Part II: Partially homogeneous environments," *IEEE Trans. Signal Process.*, vol. 62, no. 9, pp. 2358–2369, May 2014.

[20] R. S. Raghavan, N. Pulsone, and D. J. McLaughlin, "Performance of the GLRT for adaptive vector subspace detection," *IEEE Tran. Aerosp. Electron. Syst.*, vol. 32, no. 4, pp. 1473–1487, Oct. 1996.

[21] D. Pastina, P. Lombardo, and T. Bucciarelli, "Adaptive polarimetric target detection with coherent radar—Part I: Detection against gaussian background," *IEEE Tran. Aerosp. Electron. Syst.*, vol. 37, no. 4, pp. 1194–1206, Oct. 2001.

[22] A. De Maio and G. Ricci, "A polarimetric adaptive matched filter," *Signal Process.*, vol. 81, no. 12, pp. 2583–2589, Dec. 2001.

[23] J. Liu, Z.-J. Zhang, and Y. Yun, "Optimal waveform design for generalized likelihood ratio and adaptive matched filter detectors using a diversely polarized antenna," *Signal Process.*, vol. 92, no. 4, pp. 1126–1131, Apr. 2012.

[24] I. S. Reed, J. D. Mallett, and L. E. Brennan, "Rapid convergence rate in adaptive arrays," *IEEE Trans. Aerosp. Electron. Syst.*, vol. AES-10, no. 6, pp. 853–863, Nov. 1974.

[25] A. De Maio, D. Orlando, C. Hao, and G. Foglia, "Adaptive detection of point-like targets in spectrally symmetric interference," *IEEE Trans. Signal Process.*, vol. 64, no. 12, pp. 3207–3220, Dec. 2016.
[26] V. Carotenuto, A. De Maio, D. Orlando, and P. Stoica, "Model order selection rules for covariance structure classification in radar," *IEEE Trans. Signal Process.*, vol. 65, no. 20, pp. 5305–5317, Oct. 2017.
[27] Y. Gao, G. Liao, S. Zhu, X. Zhang, and D. Yang, "Persymmetric adaptive detectors in homogeneous and partially homogeneous environments," *IEEE Trans. Signal Process.*, vol. 62, no. 2, pp. 331–342, Jan. 2014.
[28] J. Liu, J. Han, Z.-J. Zhang, and J. Li, "Target detection exploiting covariance matrix structures in MIMO radar," *Signal Process.*, vol. 154, pp. 174–181, Jan. 2019.
[29] C. Hao, D. Orlando, X. Ma, and C. Hou, "Persymmetric Rao and Wald tests for partially homogeneous environment," *IEEE Signal Process. Lett.*, vol. 19, no. 9, pp. 587–590, Sep. 2012.
[30] C. Hao, D. Orlando, G. Foglia, X. Ma, S. Yan, and C. Hou, "Persymmetric adaptive detection of distributed targets in partially-homogeneous environment," *Digit. Signal Process.*, vol. 24, pp. 42–51, Jan. 2014.
[31] C. Hao, S. Gazor, G. Foglia, B. Liu, and C. Hou, "Persymmetric adaptive detection and range estimation of a point-like target," *IEEE Tran. Aerosp. Electron. Syst.*, vol. 51, no. 4, pp. 2590–2603, Oct. 2015.
[32] C. Hao, D. Orlando, G. Foglia, and G. Giunta, "Knowledge-based adaptive detection: Joint exploitation of clutter and system symmetry properties," *IEEE Signal Process. Lett.*, vol. 23, no. 10, pp. 1489–1493, Oct. 2016.
[33] J. Liu, W. Liu, H. Liu, B. Chen, X.-G. Xia, and D. Zhou, "Average SINR calculation of a persymmetric sample matrix inversion beamformer," *IEEE Trans. Signal Process.*, vol. 64, no. 8, pp. 2135–2145, Apr. 2016.
[34] L. Cai and H. Wang, "A persymmetric multiband GLR algorithm," *IEEE Tran. Aerosp. Electron. Syst.*, vol. 28, no. 3, pp. 806–816, Jul. 1992.
[35] G. Pailloux, P. Forster, J.-P. Ovarlez, and F. Pascal, "Persymmetric adaptive radar detectors," *IEEE Tran. Aerosp. Electron. Syst.*, vol. 47, no. 4, pp. 2376–2390, Oct. 2011.
[36] A. De Maio and D. Orlando, "An invariant approach to adaptive radar detection under covariance persymmetry," *IEEE Trans. Signal Process.*, vol. 63, no. 5, pp. 1297–1309, Mar. 2015.
[37] J. Liu, G. Cui, H. Li, and B. Himed, "On the performance of a persymmetric adaptive matched filter," *IEEE Tran. Aerosp. Electron. Syst.*, vol. 51, no. 4, pp. 2605–2614, Oct. 2015.
[38] J. Liu, W. Liu, Y. Gao, S. Zhou, and X.-G. Xia, "Persymmetric adaptive detection of subspace signals: Algorithms and performance analysis," *IEEE Trans. Signal Process.*, vol. 66, no. 23, pp. 6124–6136, Dec. 2018.
[39] J. Liu, W. Liu, J. Han, B. Tang, Y. Zhao, and H. Yang, "Persymmetric GLRT detection in MIMO radar," *IEEE Trans. Veh. Technol.*, vol. 67, no. 12, pp. 11913–11923, Dec. 2018.
[40] F. Gini and A. Farina, "Vector subspace detection in compound-Gaussian clutter—Part II: Performance analysis," *IEEE Tran. Aerosp. Electron. Syst.*, vol. 38, no. 4, pp. 1312–1323, Oct. 2002.
[41] F. Bandiera, O. Besson, D. Orlando, and G. Ricci, "An improved adaptive sidelobe blanker," *IEEE Trans. Signal Process.*, vol. 56, no. 9, pp. 4152–4161, Sep. 2008.
[42] F. Bandiera, D. Orlando, and G. Ricci, "A subspace-based adaptive sidelobe blanker," *IEEE Trans. Signal Process.*, vol. 56, no. 9, pp. 4141–4151, Sep. 2008.
[43] J. Carretero-Moya, A. De Maio, J. Gismero-Menoyo, and A. Asensio-Lopez, "Experimental performance analysis of distributed target coherent radar detectors," *IEEE Tran. Aerosp. Electron. Syst.*, vol. 48, no. 3, pp. 2216–2238, Jul. 2012.
[44] H.-R. Park, J. Li, and H. Wang, "Polarization-space-time domain generalized likelihood ratio detection of radar targets," *Signal Process.*, vol. 41, no. 2, pp. 153–164, Jan. 1995.
[45] D. A. Harville, *Matrix Algebra For a Statistician's Perspective*. New York, NY, USA: Springer-Verlag, 1997.
[46] E. J. Kelly and K. Forsythe, "Adaptive detection and parameter estimation for multidimensional signal models," , Lincoln Lab., Massachusetts Inst. Technol., Cambridge, MA, USA, Tech. Rep. 848, 1989.
[47] T. Anderson, *An Introduction to Multivariate Statistical Analysis*. Hoboken, NJ, USA: Wiley., 2003.
[48] A. M. Mathai and P. N. Rathie, "The exact distribution of Wilks' criterion," *Ann. Math. Statist.*, vol. 42, no. 3, pp. 1010–1019, 1971.

Jun Liu (S'11–M'13–SM'16) received the B.S. degree in mathematics from Wuhan University of Technology, Wuhan, China, in 2006, the M.S. degree in mathematics from Chinese Academy of Sciences, Beijing, China, in 2009, and the Ph.D. degree in electrical engineering from Xidian University, Xi'an, China, in 2012.

From July 2012 to December 2012, he was a Postdoctoral Research Associate with the Department of Electrical and Computer Engineering, Duke University, Durham, NC, USA. From January 2013 to September 2014, he was a Postdoctoral Research Associate with the Department of Electrical and Computer Engineering, Stevens Institute of Technology, Hoboken, NJ, USA. From October 2014 to March 2018, he was with Xidian University. He is currently an Associate Professor with the Department of Electronic Engineering and Information Science, University of Science and Technology of China, Hefei, China. His research interests include statistical signal processing, optimization algorithms, and machine learning. He is currently an Associate Editor for the IEEE SIGNAL PROCESSING LETTERS.

Siyu Sun was born in 1996. He received the B.S. degree in electronic and information engineering from HeFei University of Technology, Hefei, China, in 2018. He is currently working toward the M.S. degree in electronic and communication engineering with the University of Science and Technology of China, Hefei, China. His research interests include radar target detection and array signal processing.

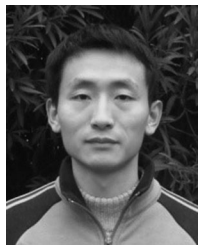

Weijian Liu (M'14) was born in Shandong, China, in 1982. He received the B.S. degree in information engineering and the M.S. degree in signal and information processing, both from Wuhan Radar Academy, Wuhan, China, and the Ph.D. degree in information and communication engineering from the National University of Defense Technology, Changsha, China, in 2006, 2009, and 2014, respectively. He is currently a Lecturer with Wuhan Electronic Information Institute, Wuhan, China. His current research interests include multichannel signal detection, statistical, and array signal processing.